The Company of Biologists

RESEARCH REPORT

Direct activation of chordoblasts by retinoic acid is required for segmented centra mineralization during zebrafish spine development

Hans-Martin Pogoda[1,*], Iris Riedl-Quinkertz[1], Heiko Löhr[1], Joshua S. Waxman[2], Rodney M. Dale[3], Jacek Topczewski[4,5], Stefan Schulte-Merker[6,7,8] and Matthias Hammerschmidt[1,9,10,*]

ABSTRACT

Zebrafish mutants with increased retinoic acid (RA) signaling due to the loss of the RA-inactivating enzyme Cyp26b1 develop a hyper-mineralized spine with gradually fusing vertebral body precursors (centra). However, the underlying cellular mechanisms remain incompletely understood. Here, we show that cells of the notochord epithelium named chordoblasts are sensitive to RA signaling. Chordoblasts are uniformly distributed along the anteroposterior axis and initially generate the continuous collagenous notochord sheath. However, subsequently and iteratively, subsets of these cells undergo further RA-dependent differentiation steps, acquire a stellate-like shape, downregulate expression of the collagen gene *col2a1a*, switch on *cyp26b1* expression and trigger metameric sheath mineralization. This mineralization fails to appear upon chordoblast-specific cell ablation or RA signal transduction blockade. Together, our data reveal that, despite their different developmental origins, the activities and regulation of chordoblasts are very similar to those of osteoblasts, including their RA-induced transition from osteoid-producing cells to osteoid-mineralizing ones. Furthermore, our data point to a requirement for locally controlled RA activity within the chordoblast layer in order to generate the segmented vertebral column.

KEY WORDS: Spine, Notochord, Chordoblast, Retinoic acid, Vertebral body, Centra, Zebrafish

INTRODUCTION

Bone forms in two principal consecutive steps: the formation of a proteinous/collagenous matrix (osteoid), and its mineralization by precipitation of calcium phosphate crystals onto the collagen fibrils (biomineralization). In tetrapods, vertebral bodies of the developing spine have a cartilaginous anlage that subsequently mineralizes or is replaced by bone, involving the consecutive action of different somite-derived cells: chondrocytes and osteoblasts, which produce the matrix/osteoid, and osteoblast-derived preosteocytes, which subsequently induce matrix mineralization (Dallas and Bonewald, 2010; Franz-Odendaal et al., 2006). In ray-finned bony fish (teleosts) such as zebrafish, vertebral body precursors (centra) develop in the absence of cartilage (Fleming et al., 2004). Here, centra form initially through mineralization of the notochord sheath, a collagen 2-based matrix deposited by outer cells of the notochord called chordoblasts (Dale and Topczewski, 2011; Grotmol et al., 2005). These segments of mineralized notochord sheath, named chordacentra, are secondarily surrounded by so-called autocentra, bone made by somite-derived scleroblasts without a cartilaginous precursor (Arratia et al., 2001; Bensimon-Brito et al., 2012; Grotmol et al., 2003; Inohaya et al., 2007).

The importance of the notochord for zebrafish centra formation was indicated over a decade ago by laser ablation experiments (Fleming et al., 2004). In addition, histological studies on salmon notochords described morphological changes and increased alkaline phosphatase expression in chordoblasts that immediately underlie the forming chordacentra, foreshadowing an implementation of this cell type in notochord sheath mineralization (Grotmol et al., 2003, 2005). Furthermore, ablation of *sp7* (also known as *osterix*)-positive osteoblasts or genetic loss of *sp7* function in zebrafish and medaka compromises the later-added autocentra and vertebral arches, but not chordacentra (Kague et al., 2016; LLeras Forero et al., 2018; Willems et al., 2012; Yu et al., 2017). Other data, however, support the importance of somite-derived scleroblasts for early steps of centra formation (Grotmol et al., 2003; Inohaya et al., 2007). In striking contrast to the vertebral column itself and the likewise segmented somites, the absence of evidence for a metameric organization of the notochord is a major limitation concerning its fundamental role in centra formation.

Here, we describe such a metameric organization of the chordoblast layer in zebrafish larvae, reflected by the segmented expression pattern of *cyp26b1*. Cyp26b1 is an enzyme of the cytochrome P450 family that oxidizes the paracrine signaling molecule *all-trans* retinoic acid (RA) to biologically inactive metabolites (Pennimpede et al., 2010). Zebrafish *cyp26b1* loss-of-function mutants display excessive biomineralization along the notochord, eventually resulting in fused centra formation, as also induced in wild-type zebrafish and to some extent in mice by administration of exogenous RA or a chemical Cyp26 inhibitor (Laue et al., 2008; Spoorendonk et al., 2008). This indicates that RA inhibition by Cyp26 enzymes is an evolutionarily conserved mechanism to prevent RA from spreading into prospective intervertebral spaces, thereby ensuring strictly metameric centra positioning. However, the precise cellular mechanisms of RA-dependent centra formation remain elusive.

[1]Department of Biology, Institute of Zoology – Developmental Biology, University of Cologne, 50674 Cologne, Germany. [2]Molecular Cardiovascular Biology Division, Cincinnati Children's Hospital Medical Center, Cincinnati, OH 45229, USA. [3]Department of Biology, Loyola University Chicago, Chicago, IL 60660, USA. [4]Department of Pediatrics, Northwestern University Feinberg School of Medicine, Chicago, IL 60611-2605, USA. [5]Department of Biochemistry and Molecular Biology, Medical University of Lublin, 20-093 Lublin, Poland. [6]Institute of Cardiovascular Organogenesis and Regeneration, Faculty of Medicine, 48149 Münster, Germany. [7]CiM Cluster of Excellence (EXC-1003), WWU Münster, 48149 Münster, Germany. [8]Hubrecht Institute – KNAW & UMC Utrecht, 3584CT Utrecht, Netherlands. [9]CECAD Cluster of Excellence, University of Cologne, 50931 Cologne, Germany. [10]Center for Molecular Medicine Cologne (CMMC), University of Cologne, 50931 Cologne, Germany.

*Authors for correspondence (pogodah@uni-koeln.de; mhammers@uni-koeln.de)

H.-M.P., 0000-0003-3196-1720; J.S.W., 0000-0002-8132-487X; R.M.D., 0000-0003-4255-4741; J.T., 0000-0001-6023-9556; S.S.-M., 0000-0003-3617-8807; M.H., 0000-0002-3709-8166

Received 15 September 2017; Accepted 29 March 2018

DEVELOPMENT

Recently, we showed that in calvaria, the flat bones of the skull, RA promotes ossification by stimulating the transitioning of osteoblasts to preosteocytes, thereby terminating osteoid production and initiating osteoid mineralization (Jeradi and Hammerschmidt, 2016; Laue et al., 2011). Here, we provide evidence for an equivalent mode of RA action during chordacentra formation around the notochord. In this case, however, RA acts on chordoblasts of the notochord as the direct target cells and essential effectors. As chordoblasts per se are uniformly distributed along the anteroposterior axis, our data also point to locally active RA as a mechanism accounting for the metameric organization of the developing chordacentra.
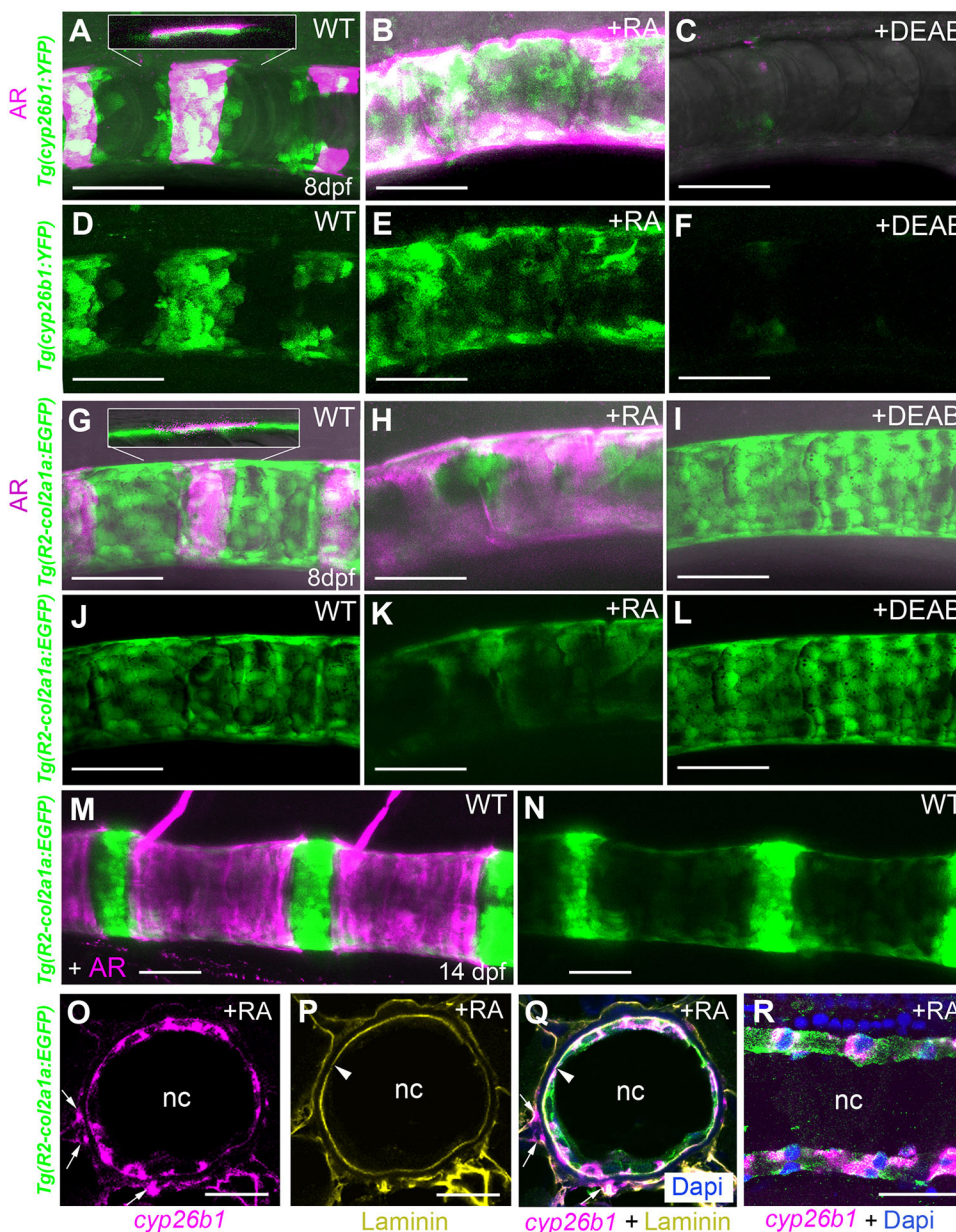
RESULTS AND DISCUSSION

Chordoblasts of the notochord respond to retinoic acid with increased Cyp26b1 and reduced type II collagen production

Cyp26 genes are known direct transcriptional targets of RA signaling, accounting for negative feedback regulation (Pennimpede et al., 2010). Therefore, we generated a transgenic $cyp26b1:YFP^{hu7426}$ line to identify potential RA-receiving cells in the context of centra formation in zebrafish. At 8 days post-fertilization (dpf) segmented clusters of YFP-positive cells were found in close association with developing, Alizarin Red (AR)-positive centra (Fig. 1A,D). These reiterative YFP- and AR-positive domains expanded and fused upon treatment of larvae from 4 dpf onwards with exogenous RA (Fig. 1B,E). In contrast, transgene expression and centra mineralization were lost upon corresponding treatment with DEAB (N,N-diethylaminobenzaldehyde), a chemical inhibitor of RA synthesis (Fig. 1C,F). This indicates that the $cyp26b1:YFP$ transgene does indeed respond to RA either directly or indirectly. Closer inspection revealed that these YFP-positive cells had a flat shape and were not localized at the outer surface of the mineralized notochord sheath (as one might expect for somite-derived scleroblasts/osteoblasts), but at their inner surface, identifying them as chordoblasts (Fig. 1A, inset).

The teleostean notochord consists of two distinct cell types: the centrally arranged vacuolated cells that make up the main part of this

Fig. 1. Centra-associated subsets of otherwise uniformly distributed chordoblasts express *cyp26b1* in an RA-dependent manner. (A-N) Lateral views of notochords at the level of centra 3-5 in control (A,D, *n*=67; G,J, *n*=72; M,N, *n*=10), RA-treated (B,E, *n*=84/84; H,K, *n*=53/53) or DEAB-treated (C,F, *n*=77/77; I,L, *n*=32/32) larvae bearing the indicated YFP- or GFP-encoding transgenes. Anterior is to the left; calcified extracellular matrix is labeled by Alizarin Red. (A-C,G-I,M) Projections of confocal stacks with merged green, magenta and transmitted light channels. (D-F,J-L,N) Corresponding single green channel projections. Insets (A,G) show single confocal planes, revealing that YFP- and GFP-positive cells are located on the inner surface of the mineralized notochord sheath. (O-R) Fluorescence *in situ* hybridization of *cyp26b1* transcripts on transverse (O-Q; level of chordacentra) and sagittal (R) sections through the notochord, co-labeled by immunofluorescence against Laminin (yellow) and *Tg(R2-col2a1a: EGFP)*-encoded EGFP (green). Arrowheads highlight notochord basement membrane, arrows *cyp26b1*-positive cells outside the notochord, possibly representing somite-derived scleroblasts generating the outer autocentra (Bensimon-Brito et al., 2012). Scale bars: 50 µm (A-N); 20 µm (O-R). AR, Alizarin Red; nc, notochord; WT, DMSO/ethanol-treated wild-type control.

structure, and an outer monolayer of flat chordoblasts, sometimes also referred to as notochord epithelium cells or notochord sheath cells. These chordoblasts express the *col2a1a* gene [Fig. 1O-R, co-expression of transgenic *col2a1a:EGFP* with a chordoblast-specific R2 driver (Dale and Topczewski, 2011) and *cyp26b1*] and secrete material for the notochord sheath, a collagen 2-based envelope enwrapping the notochord (Grotmol et al., 2005). Like the central vacuolated cells, chordoblasts derive from the notochord anlage, as indicated by former cell-tracking studies (Dale and Topczewski, 2011), and as confirmed by our own lineage-tracing experiments for *cyp26b1*-positive chordoblasts, using an early axial mesoderm-specific *goosecoid* driver (Doitsidou et al., 2002) (Fig. S1).

In contrast to the *cyp26b1:YFP* expression domains (Fig. 1A,D), chordoblasts, as identified by the *R2-col2a1a:EGFP* transgene, are not organized in a metameric manner, but uniformly distributed along the entire anteroposterior notochord axis (Fig. 1G,J; Fig. S2A,B). Hence, the segmented expression of *cyp26b1* depicts only a subset of chordoblasts. Furthermore, in contrast to the negative response of *cyp26b1:YFP* to the RA inhibitor DEAB (Fig. 1C,F) and its positive response to RA (Fig. 1B,E), DEAB did not affect *R2-col2a1a:EGFP* (Fig. 1I,L), while RA progressively downregulated *R2-col2a1a: EGFP* transgenic expression (Fig. 1H,K), concomitant with progressive alterations in chordoblast cell shapes from roundish and compact to more irregular with less distinct cell borders (Fig. S2). Weaker *R2-col2a1a:EGFP* transgene activity was also observed in chordoblasts of 14 dpf untreated larvae immediately underneath further developed centra (Fig. 1M,N). Together, these data suggest that endogenous RA in a reiterative fashion affects only subsets of chordoblasts, leading to a metameric anteroposterior pattern within this notochordal cell population. Furthermore, RA stimulation of chordoblasts reduces their collagen production, thereby attenuating notochord sheath formation (see also Fig. 3). This negative effect on collagen synthesis is remarkably similar to the previously observed effect of RA on osteoblasts in the zebrafish skull, one aspect of the promoted osteoblast-to-preosteocyte transitioning that we have recently described (Jeradi and Hammerschmidt, 2016; Laue et al., 2011).

Chordoblasts respond to retinoic acid with increased biomineralizing activity

To study whether RA-stimulated chordoblasts also gained properties comparable to those of preosteocytes, we carried out *in situ* hybridizations and qRT-PCR analyses for *entpd5a* transcripts as a marker for biomineralizing activity (Huitema et al., 2012). By hydrolyzing nucleoside triphosphates, Entpd5 locally provides inorganic monophosphate for biomineralization, a function dedicated to preosteocytes of 'regular' bone (Dallas and Bonewald, 2010; Franz-Odendaal et al., 2006). In zebrafish, Entpd5a function is crucial for bone formation, and *entpd5a* mutants lack all bone (Huitema et al., 2012). Indeed, double-labeling experiments revealed that zebrafish *entpd5a* was expressed in *cyp26b1*-positive chordoblasts (Fig. 2A-F). In wild type, *entpd5a* expression was metameric (Fig. 2C,F,G), in agreement with an independent study showing *entpd5a* expression next to forming centra in an *entpd5a* transgenic line (LLeras Forero et al., 2018), while it appeared to be expanded, stronger and often even fused in RA-treated, but abolished in DEAB-treated, larvae (Fig. 2G-J). Furthermore, induction of *entpd5a* expression by RA treatment was as rapid as that of *cyp26b1*, with almost 4-fold increased transcript levels within 1 h of RA addition (Fig. 2K). Together, these data suggest that RA induces chordoblasts to produce both Entpd5a and Cyp26b1, the latter to
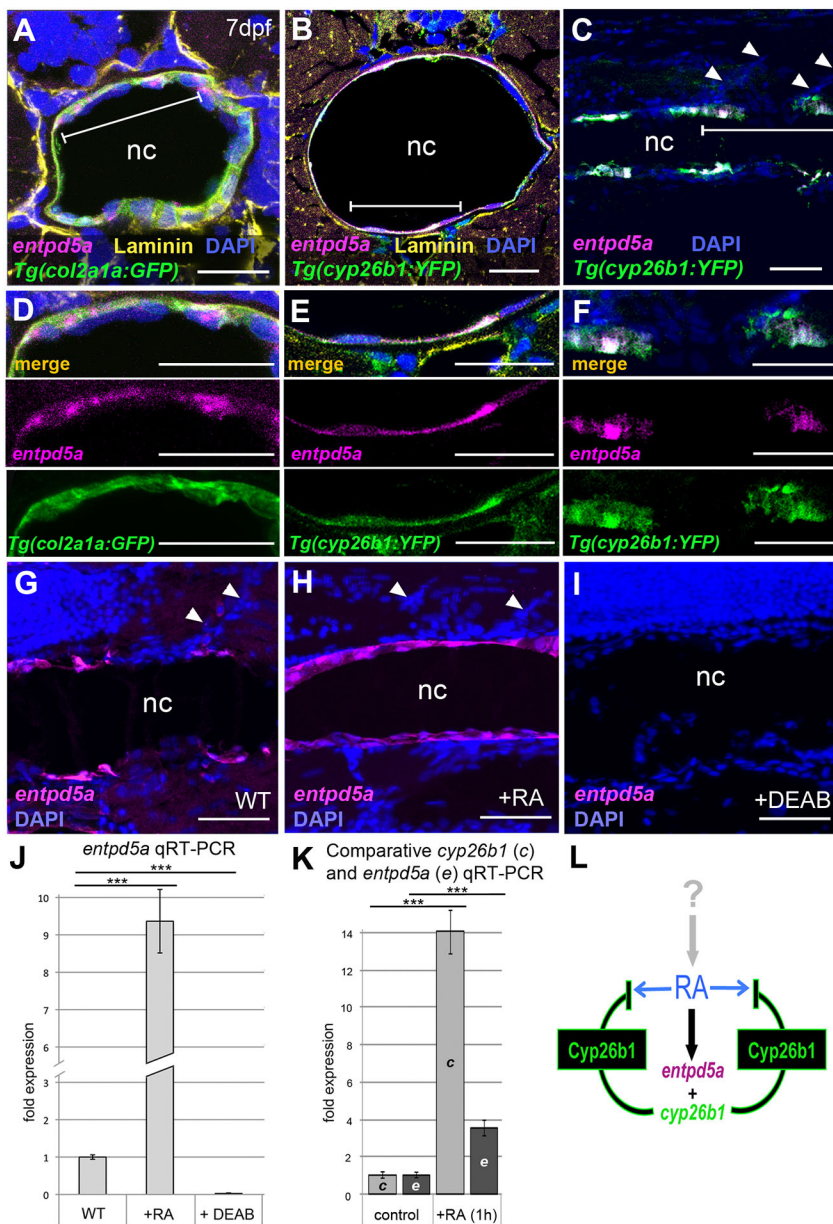
inactivate RA, thereby compromising RA spreading into prospective intervertebral spaces and spatially restricting the transitioning of chordoblasts to biomineralizing cells (Fig. 2L). Consistent with these findings, transmission electron microscopy (TEM) revealed that upon RA treatment chordoblasts acquired a more stellate-like morphology (Fig. 3A,B) with markedly reduced rough endoplasmic reticulum (Fig. 3E,F), which are typical characteristics of preosteocytes (Dallas and Bonewald, 2010; Franz-Odendaal et al., 2006; Laue et al., 2011). Furthermore, in line with the reduction of the rough endoplasmic reticulum and downregulation of collagen expression (Fig. 1), the notochord sheath of RA-treated and *cyp26b1* mutant animals was slightly, but significantly, thinner (Fig. 3C,D,G), pointing to reduced secretory and sheath-forming activity of such chordoblasts. Taken together, despite their different embryonic origin, chordoblasts react to RA in a similar manner to osteoblasts during intramembranous bone formation (Laue et al., 2011), reducing their matrix-generating activity and promoting notochord sheath mineralization and, thereby, chordacentra formation.

Chordoblasts are required for chordacentra formation

To test whether chordoblasts are indeed required for chordacentra formation, we next genetically ablated chordoblasts in a temporally controlled fashion, employing the nitroreductase (Ntr)–metronidazole (Mtz) system (Curado et al., 2007; Willems et al., 2012). A requirement of the notochord for centra formation had formerly been addressed, using laser ablation technology (Fleming et al., 2004). However, in this case, (presumably) both central vacuolated cells and peripheral chordoblasts had been ablated and the notochord sheath was likely damaged as well. In contrast, using the transgenic *R2-col2a1a* driver enabled us to ablate chordoblasts specifically. In the absence of Mtz, untreated *col2a1a:CFP-NTR* transgenic larvae displayed reiterative axial mineralization (Fig. 4A, A′), whereas RA treatment caused hyper-mineralization (Fig. 4B) as in non-transgenic fish (Fig. 1G,H). However, exposure to 7 mM Mtz from 4 to 6.5 dpf strongly disrupted the chordoblast layer, as reflected by severely compromised reporter transgene expression (Fig. 4A,C) and the absence of distinct chordoblasts in transmission electron micrographs (Fig. S3E,F). Vacuolated notochord cells remained intact (Fig. S3A-D). Strikingly, the notochord sheath, although of only moderately reduced thickness (Fig. 4E-G), completely failed to mineralize (Fig. 4C,C′), an effect that could not be reversed upon RA treatment (Fig. 4D). Only at 16 dpf, 9.5 days after the end of chordoblast ablation, could small centra and outgrowing neural arches be observed in treated animals (Fig. S4), coinciding with the recovery of the chordoblast population. Together, these observations indicate that chordoblasts have widely diminished notochord sheath formation by 4 dpf, but are later absolutely essential for sheath mineralization and thus chordacentrum formation.

Chordoblasts are direct cellular targets of retinoic acid

Finally, to study whether the effect of RA on sheath mineralization involves direct RA signaling to chordoblasts, we generated a *col2a1a:EGFP-dnRARa* transgenic line for chordoblast-specific expression of a dominant-negative version of the human RA receptor alpha, fused to EGFP. *col2a1a:EGFP-dnRARa* construct-injected G0 animals with mosaic expression lacked notochord sheath mineralization in regions with EGFP-positive chordoblasts, whereas in regions devoid of EGFP signal, thus containing wild-type chordoblasts, the sheath showed Alizarin Red staining (Fig. 4H,I). Non-mosaic individuals from a stable transgenic line displayed a complete loss of notochord sheath mineralization, even though the

Fig. 2. *cyp26b1*-positive chordoblasts co-express the biomineralization gene *entpd5a* in an RA-dependent manner. (A-I) *In situ* hybridization for *entpd5a* transcripts (magenta) on transverse (A,B,D,E; level of chordacentra) or sagittal (C,F,G-I) notochord sections of wild-type (A-F), control- (G), RA- (H) or DEAB-treated (I) larvae at 7 dpf, co-labeled with DAPI (blue), anti-Laminin (yellow), anti-*Tg(R2-col2a1a:EGFP)*-derived EGFP (green) and/or anti-*Tg(cyp26b1:YFP)*-derived YFP immunofluorescence (green). (D-F) Magnifications of the areas demarcated by brackets in A-C. Upper panels of D-F show cognate images of merged channels, middle and lower panels single channel images for *entpd5a* expression (magenta) and anti-GFP or anti-YFP immunofluorescence (green), respectively. Scale bars: 20 µm (A,B,D,E); 50 µm (C,F,G-I). Arrowheads (C,G,H) indicate somite borders. (J) qRT-PCR analysis of *entpd5a* transcript levels in trunks of 7 dpf larvae after 3 days of RA or DEAB treatment (*n*=30 per condition); mean±s.d.; ***P<0.0001. (K) qRT-PCR analysis of *cyp26b1* and *entpd5a* transcript levels in trunks of 5 dpf larvae after 1 h of RA treatment (*n*=20 per condition); mean±s.d.; ***P<0.0001. (L) Schematic model of the molecular events at a forming chordacentrum: RA, generated and regulated by thus far unknown cells and upstream factors, co-induces chordoblast-specific expression of *entpd5a* and *cyp26b1*. Cyp26b1 enzyme inactivates RA at its site of action to restrict lateral spreading of the signal and to ensure physiologically appropriate RA concentrations. nc, notochord.

transgene was more weakly expressed (Fig. 4J). In addition, *col2a1: EGFP-dnRARa*; *cyp26b1:YFP* double-transgenics displayed a widespread loss of the YFP signal in chordoblasts, indicating absence of RA target gene activation. In contrast, YFP expression was maintained in potential scleroblasts (see also Fig. 1O,Q) at the outer surface of the notochord sheath (Fig. 4K-N). This strongly suggests that the transgene-encoded dominant-negative receptor only has cell-autonomous effects, identifying the chordoblasts as direct RA target cells.
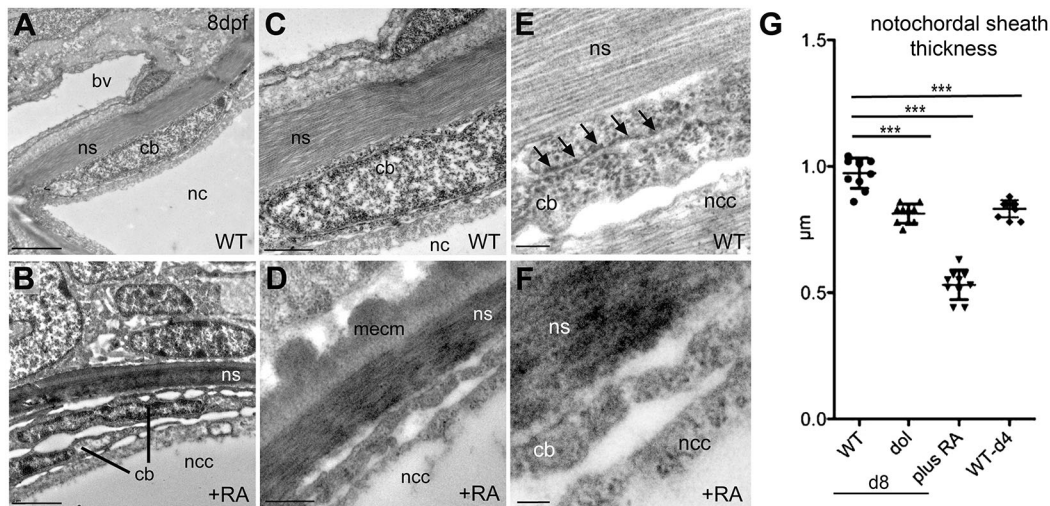
Chordoblasts and their regulation by retinoic acid play crucial roles during axial skeleton formation and segmentation

In summary, these data identify the chordoblasts of the notochord as the key skeletogenic cells during chordacentrum development, helping to clarify a long-standing debate about the origins of chordacentra (Fleming et al., 2004, 2015; Grotmol et al., 2005; Kague et al., 2016; Owen, 1866; Willems et al., 2012; Yu et al., 2017). Initially generating the notochord sheath, they are later

stimulated by RA signals to differentiate further into biomineralizing cells to drive metameric sheath mineralization, comparable to the roles and regulation of osteoblasts and their transitioning to preosteocytes during osteoid mineralization in 'regular' bone. Of note, chordoblasts generate collagen 2, as is typical for cartilage, rather than collagen 1, as is typical for bone. In this light, their transition to biomineralizing cells is even more similar to that of chondrocytes in mineralizing cartilages in health and disease (Anderson, 2003; Bertrand et al., 2010).

It is noteworthy that the key step in initial mineralization of chordacentra is the expression of *entpd5a* in a metameric pattern along the anteroposterior axis (LLeras Forero et al., 2018; Wopat et al., 2018). These observations, and data presented here, provide direct evidence for a metameric organization of such mineralizing chordoblasts along the anteroposterior axis of the zebrafish larva, a crucial prerequisite for a fundamental role of the notochord in setting up the segmented vertebral column and consistent with previous observations in salmon (Grotmol et al., 2003). Future studies will be required to elucidate the mechanisms underlying the

Fig. 3. Chordoblasts of RA-treated zebrafish larvae acquire preosteocyte-like morphological features. (A-F) Transmission electron micrographs of transverse sections through the notochord of control- (A,C,E; level of prospective intervertebral spaces) and RA-treated (B,D,F) larvae at 8 dpf. Scale bars: 2 μm (A,B); 0.5 μm (C,D); 0.1 μm (E,F). Note the higher electron density of the notochord sheath in B and D, indicative of its strong mineralization. bv, blood vessel; cb, chordoblast; mecm, mineralized extracellular matrix; nc, notochord; ncc, notochordal cell; ns, notochordal sheath. Arrows in E point at a stretch of rough endoplasmic reticulum, which is barely found in chordoblasts of RA-treated larvae (F). (G) Quantification of notochord sheath thickness in different genetic backgrounds or after RA treatment as indicated; $n=10$ per condition; mean±s.d.; ***$P<0.0001$. dol, $cyp26b1^{ti230g}$ mutant (*dolphin*) (Laue et al., 2008). At 8 dpf (d8), the mutant shows reduced thickness of the notochord sheath, comparable to the thickness of wild types at 4 dpf (d4), most likely due to the premature reduction of sheath formation in chordoblasts. In wild-type larvae treated with RA from 4 to 8 dpf, the width of the sheath is even more strongly reduced, possibly pointing to additional RA-induced active sheath resorption (compare with Jeradi and Hammerschmidt, 2016; To et al., 2012).

acquisition of this metameric chordoblast pattern. Interfering with segmentation clock activity in the paraxial mesoderm has little effect on the metameric *entpd5a* pattern in the notochord (LLeras Forero et al., 2018), although recently a role for intrinsic Notch signaling has been proposed (Wopat et al., 2018). Another simple explanation would be a segmentally provided RA source. Chordoblasts in close proximity to these thus far unidentified metameric RA sources would not only respond to RA by driving sheath mineralization, but would also start to generate Cyp26b1 to inactivate RA. This would thereby prevent RA from reaching more remote chordoblasts, ensuring the persistence of the intervertebral domains. In contrast, genetic loss of Cyp26b1 in *dolphin*/*stocksteif* mutants would lead to spreading of RA and to hyper-mineralization in the axial skeleton. Consistently, in these mutants the initial mineralization steps appear to be patterned normally, with lack of Cyp26b1 activity only gradually leading to mineralization of regions adjacent to chordacentra (Laue et al., 2008; Spoorendonk et al., 2008). This ectopic activation of chordoblasts and the corresponding mineralization in the normally non-mineralized intervertebral notochord sheath domains in *cyp26b1* mutants also indicates that all chordoblasts are, in principle, competent for RA signal reception. Thus, they should not differ in their RA receptor or RA-binding protein contents.

Future studies are needed to resolve the extent to which chordoblasts are also involved in centra formation in other vertebrates. Of note, collagenous notochord sheaths made by notochordal cells, and chordacentra or perichordal centra formed within or around reiterative notochord sheath areas, are found in all clades of gnathostomes (jawed vertebrates), including tetrapods (Fleming et al., 2015; Paavola et al., 1980; Scaal, 2016). However, in cartilaginous fish, lungfish and tetrapods, the chorda- and perichordal centra are formed from cartilaginous templates, which are thought to be generated and ossified by somite-derived scleroblasts that either invade the notochordal sheath or tightly

associate with its outer surface. However, this model does not rule out a parallel action of chordoblasts from the inner side of the sheath. Conversely, the essential role of chordoblasts during chordacentrum formation in teleosts, as reported here, does not rule out a simultaneous and supportive action by scleroblasts, consistent with the presence of RA-responsive, *cyp26b1*- and *col10*-expressing (Laue et al., 2008; Renn et al., 2013) and sclerotome-derived (Inohaya et al., 2007) cells at the outer surface of the notochord sheath in zebrafish and medaka larvae.
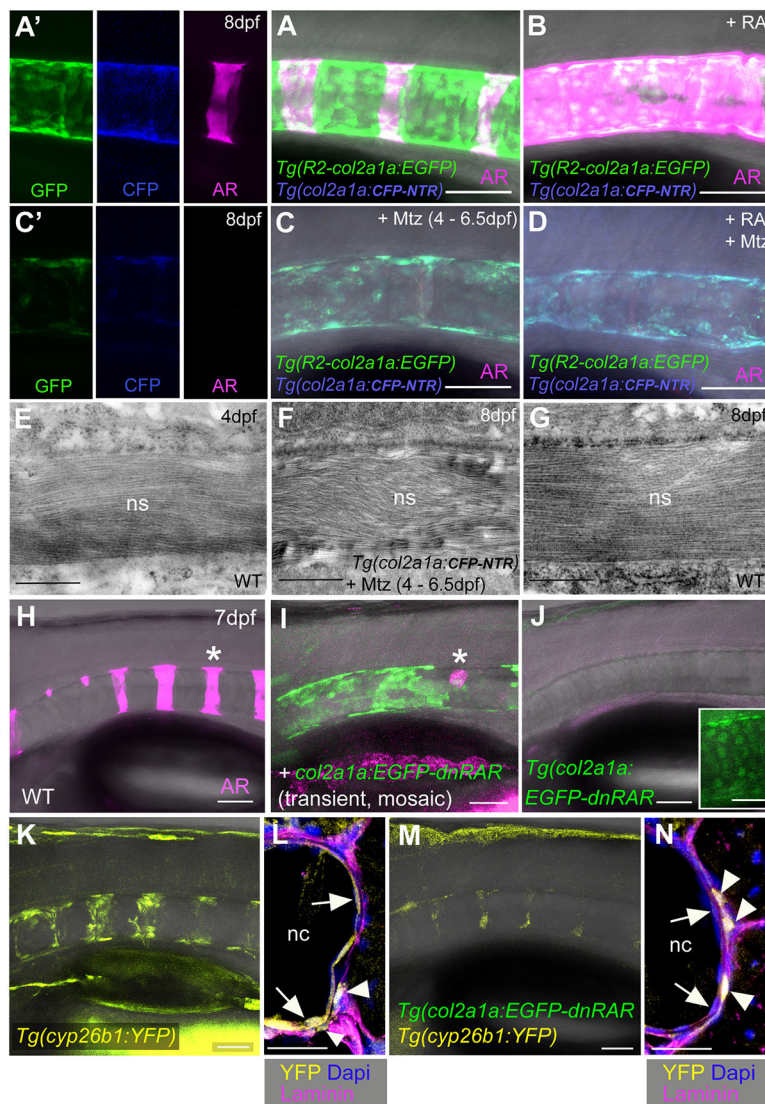
MATERIALS AND METHODS
Zebrafish lines
The following zebrafish lines were used: $Tg(R2\text{-}col2a1a:EGFP)^{nu13Tg}$ (Dale and Topczewski, 2011) and $Tg(hsp70:loxp\text{-}dsred\text{-}loxp\text{-}egfp)^{tud107Tg}$ (Kroehne et al., 2011). The $Tg(cyp26b1:YFP)^{hu7426}$, $Tg(col2a1a:CFP\text{-}NTR)^{fr42Tg}$, $Tg(col2a1a:EGFP\text{-}Hs\text{-}dnRARa)^{fr43Tg}$, $Tg(gsc:Cre)^{fr44Tg}$ and $Tg(bact2:loxP\text{-}AmCyan\text{-}loxP\text{-}mCherry)^{fr45Tg}$ lines were generated in the course of this study (see below for details). Requests for $Tg(cyp26b1:YFP)^{hu7426}$ should be directed to S. Schulte-Merker. All zebrafish experiments were approved by the local and federal animal care committees in Cologne (LANUV Nordrhein-Westfalen; 8.87-50.10.31.08.129; 84-02.04.2012.A251; 84-02.04.2012.A390; City of Cologne; 576.1.36.6.3.01.10 Be) and the Netherlands (DEC committee).

RA, DEAB and Mtz treatments
Stock solutions (10 mM) of DEAB (Sigma-Aldrich) and *all-trans* RA (Sigma-Aldrich) in DMSO as well as the corresponding working dilutions (for concentrations see below) were prepared as described (Begemann et al., 2004). Wild-type or transgenic zebrafish larvae were incubated with final concentrations of 1 μM RA or 10 μM DEAB from 4 dpf until phenotypic evaluation or RNA extraction at 7 dpf or 8 dpf. As controls, siblings were treated with equivalent concentrations of ethanol/DMSO or DMSO alone. Metronidazole (Mtz; Sigma-Aldrich) solution was freshly prepared in embryo medium. For chordoblast ablation, larvae were treated with 7 mM Mtz from 4 dpf until 6.5 dpf. For parallel treatment with RA, larvae were exposed to a cocktail of 7 mM Mtz/1 μM RA between 4 dpf and 6.5 dpf

Fig. 4. Biomineralization of the notochord sheath is impaired upon chordoblast-specific cell ablation or RA reception inhibition. (A-D) Lateral views of notochords at the level of centra 3-5 in control-treated (A, *n*=42), RA-treated (B, *n*=25), Mtz-treated (C, *n*=63/63) and RA+Mtz-treated (D, *n*=47/47) *R2-col2a1a:EGFP; col2a1a:CFP-NTR* double transgenics at 8 dpf; confocal projections with merged green (GFP), magenta (Alizarin Red), blue (CFP-NTR) and transmitted light channels; panels A′ and C′ show single channels of middle parts of A and C, respectively. (E-G) Transmission electron micrographs of transverse sections through the notochord sheath at the level of chordacentra of untreated larvae at 4 dpf (E, *n*=5) or 8 dpf (G, *n*=5), and of Mtz-treated *R2-col2a1a:EGFP; col2a1a:CFP-NTR* double-transgenic at 8 dpf (F, *n*=6). The final width of the notochord sheath has almost been reached at 4 dpf and is not significantly affected by chordoblast ablation via Mtz administration between 4 and 6.5 dpf (compare F and G). (H-K,M) Lateral views of notochords from larvae with the indicated genotypes at 7.5 dpf, levels of centra 1-6, anterior to the left. (H-J) Projections of confocal stacks with merged magenta (Alizarin Red), green (transgene-encoded EGFP-dnRARa) and transmitted light (H, *n*=25; I, *n*=14/14; J, *n*=45/47) channels. Asterisk in I indicates region devoid of EGFP-dnRARa-positive cells that corresponds to centrum #5 in wild type (asterisk in H). Inset in J shows a magnified view of a portion of the notochord with gained intensity of the green channel, revealing nuclear EGFP-Hs-dnRARa fusion protein. (K,M) Stacks of merged yellow (transgene-encoded YFP) and transmitted light (K, *n*=38; M, *n*=42/42) channels. (L,N) Immunofluorescence staining on transverse sections through notochords at level of chordacentra from specimens with genotypes as in K and M and with antigen labeling as indicated. Scale bars: 0.5 µm (E-G); 50 µm (A-D,H-K,M); 20 µm (L,N). Arrows in L and N point to chordoblast layer, arrowheads to labeled cells outside the notochord [WT, *n*=6; *Tg(col2a1a:EGFP-dnRAR)*, *n*=4; ratio of *Tg(cyp26b1:YFP)*-positive cells inside and outside the notochord: 26/10 (WT), 3/16 (Tg)]. AR, Alizarin Red; nc, notochord; ns, notochord sheath.

followed by incubation in 1 µM RA alone from 6.5 dpf until 8 dpf. All drug treatments were carried out in the dark in a 28°C incubator.

Plasmid construction and transgenesis

The *Tg(cyp26b1:YFP)^hu7426* transgene was generated by standard procedures (Bussmann and Schulte-Merker, 2011) using a BAC construct that had previously been reported to serve as a read-out for *cyp26b1* expression (Spoorendonk et al., 2008). The plasmids for generation of the *Tg(col2a1a:CFP-NTR)*, *Tg(col2a1a:EGFP-Hs-dnRARa)*, *Tg(bact2:loxP-AmCyan-loxP-mCherry)* and *Tg(gsc:Cre)* lines were cloned using the Multistep Gateway Recombineering system (Invitrogen) and the Tol2kit (Kawakami and Shima, 1999; Kwan et al., 2007); primers used are listed in Table S1. For construction of the cognate p5E *col2a1a* R2-E1b plasmid, we utilized *Tg(col2a1a:EGFP)* (ZFIN ID: ZDB-TGCONSTRCT-111205-2) as a template (Dale and Topczewski, 2011). The *col2a1a* R2 regulatory element and E1B minimal promoter sequences were amplified separately and the presence of single proper bands (at 387 bp and 89 bp, respectively) was confirmed, then PCR products were column purified. The R2 and E1b fragments were mixed at equal molar ratios and ligated together at room temperature using T4 DNA Ligase (New England Biolabs) for 1.5 h. One-tenth of the ligation reaction was then used in a standard Gateway BP reaction with the pDONR4-1 vector. Desired clones were selected, propagated and sequenced to check for construct integrity. An ~80 bp insertion of an extra E1b minimal promoter was identified in the best clone.

To correct this, the plasmid was cut with *Bsp*1407I (Fermentas), which completely removed the extra inserted E1b minimal promoter fragment, and then re-transformed. For the generation of a p5E-*gsc* vector, a 2 kb *gsc*-promoter element (PMID: 8734495) was amplified from genomic DNA and subcloned into pBluescript. From here, the promoter was excised using *Xho*I and *Sma*I (both New England Biolabs) and ligated into an *Xho*I/*Sma*I-linearized universal 5′-entry vector p5E-MCS (Kwan et al., 2007). pME-*CFP-NTR* and pME-*Cre* were generated by addition of attB1-B2 attachment sites to a *CFP-NTR* fusion construct or to a *Cre* open reading frame by PCR followed by a BP reaction for the insertion into pDONR 221. For the construction of the fusion between EGFP and a dominant-negative variant of *Homo sapiens* retinoic receptor RARa cDNA, EGFP cDNA including a linker sequence encoding ESLGDLT was fused to the 5′ end of the previously reported human dnRARa cDNA (Waxman and Yelon, 2011) by PCR. The EGFP-dnRARa fusion cDNA was subsequently cloned into the pDONR 221 middle entry clone via BP reaction. To confirm that the fusion protein was functional, stable transgenic lines (not used further in this study) incorporating the *hsp70l* promoter to drive EGFP-dnRARa expression were generated with Tol2. Following heat-shock induction at the sphere stage, transgenic embryos expressed GFP and exhibited overt phenotypes, such as enlarged hearts and loss of forelimbs, which are consistent with loss of RA signaling (Waxman and Yelon, 2011) (data not shown). All 5′- and middle entry plasmids were sequenced to check for construct integrity. Finally, cognate 5′- and middle entry plasmids were combined with p3E-pA (Kwan

et al., 2007) and the destination vector pDestTol2CG2 (Kwan et al., 2007) by LR reactions. For the generation of the *Tg(bact2:loxP-AmCyan-loxPmCherry)* transgenic line, the Gateway-compatible plasmid p5E-bact2 containing the medaka *β-actin* (*bact2*) promoter (Chou et al., 2001) was generated. For this purpose, a 3.7 kb *bact2* promoter fragment was amplified by PCR from plasmid *β-actin:mGFP* (Cooper et al., 2005). The primers used (see Table S1 for sequences) carried cognate 5′-attB4/1 sites for subsequent BP recombination, which was performed together with pDONR-P4-P1R as target vector (Kwan et al., 2007). The resultant p5E-bact2 plasmid was in turn assembled with pME-loxP-AmCyan-loxP (Zhou et al., 2011), p3E-mCherry and pDestTol2pA2 using LR Gateway cloning. Mosaic G0 larvae (Fig. 4A-B) and stable transgenic lines (Fig. 3A-D, Fig. 4C-G, Fig. S1) were generated by standard injection and screening procedures.

Tissue cryosectioning, *in situ* hybridization and immunohistochemistry
Cryosectioning and fluorescence *in situ* hybridization with 555 nm TSA substrate followed by immunofluorescence (IF) staining were carried out as described (Jeradi and Hammerschmidt, 2016; To et al., 2012) with two modifications: tissue slices were prepared at a thickness of 10 μm, and hybridization was carried out at 60°C. Digoxygenin-labeled probe for *cyp26b1* was prepared as described (Laue et al., 2008). For generation of *entpd5a* probe, a 1.3 kb partial cDNA sequence was isolated from wild-type 48 hpf cDNA by PCR, cloned into pCRII (Invitrogen) and transcribed (see supplementary Materials and Methods). Subsequent IF stainings were performed with the primary antibodies chicken anti-GFP (Thermo Fisher Scientific, A-10262) and rabbit anti-Laminin (Sigma, L9393), and the secondary antibodies Alexa Fluor 488-conjugated goat anti-chicken (Thermo Fisher Scientific, A-11039) and Alexa Fluor 647-conjugated goat anti-rabbit (Thermo Fisher Scientific, A-21244). Primary antibodies were used at 1:500 and secondary antibodies at 1:1000 in block solution [10% calf serum, 1% dimethyl sulfoxide (Sigma), 0.3% Triton X-100 in PBS].

Imaging
Confocal *z*-stacks were recorded using a Zeiss LSM 710 microscope. Fluorescent signals were excited by appropriate wavelengths of a one-photon laser and detected sequentially in separate channels. For *in vivo* confocal imaging, whole larvae were anesthetized with 1× Tricaine (0.16 mg/ml embryo medium) and mounted in 1.5% low melting agarose/1×Tricaine in embryo medium. For subsequent image processing, ZEN 2008 (Zeiss) and Photoshop CS2 (Adobe) software were used.

TEM analysis
For TEM, zebrafish larvae were fixed in 2.5% glutaraldehyde in PBS for 30 min at room temperature and then at 4°C overnight. Fixed specimens were then washed several times in PBS and twice in 0.1× PBS, post-fixed with 1% osmium tetroxide in 0.1× PBS for 1 h at 4°C, washed three times in 0.1× PBS and incubated in 1% uranyl acetate for 30 min at 4°C, dehydrated in a graded series of ethanol, and embedded in Araldite (Hundsman Advanced Materials). Ultrathin sections (70 nm) were cut using the ultramicrotome Leica EM UC7, mounted on Pioloform-covered copper grids and post-stained with aqueous uranyl acetate (2%, 10 min) and Reynolds' lead citrate (3.5 min). The samples were examined with a CM 10 transmission electron microscope (FEI Europe). Micrographs were taken with the ORIUS SC200W TEM CCD camera using the software DigitalMicrograph (Gatan), which was also used for micrograph internal measurements.

Alizarin Red and calcein *in vivo* stains
Alizarin Red and calcein stains on living larvae were performed as described (Jeradi and Hammerschmidt, 2016; To et al., 2012), with the slight modification that the working solutions had a concentration of 50 mg/l of embryo medium. For the phenotypic evaluation of notochord sheath mineralization, the domain of centrum #1 to centrum #6 was analyzed in this study.

qRT-PCR
Per condition, total RNA from 30 7-dpf (Fig. 2J) or 20 5-dpf (Fig. 2K) larvae (decapitated posterior to the inner ear) was isolated using Trizol Reagent

(Thermo Fisher Scientific) with the PureLink RNA Mini Kit (Thermo Fisher Scientific), including on-column DNaseI treatment followed by reverse transcription with Superscript II reverse transcriptase (Thermo Fisher Scientific). Gene expression was assayed by qRT-PCR with an ABI-PRISM 7500 Fast Detection system and TaqMan assays (*cyp26b1*: premade assay Dr03088547_m1; *entpd5a*: custom-made assay, forward primer A-GCCCGGACTGTCAGCATAT, reverse primer TCAACAGCTGCACAA-TGGATTC, probe primer TATGCCTGAAAAGGGTGG), normalized against *rps23* (Assay ID Dr03430371_m1), and with technical triplicates of each sample. Relative differences were calculated using the $\Delta\Delta C_T$ method. Mean values and standard deviations were determined with Excel software. One representative experiment is shown in Fig. 2J,K. However, very similar results were obtained with three independent biological samples per condition.

Statistics
Statistical analyses were performed using Prism7 software (GraphPad Software). Significance between groups was determined using unpaired Student's *t*-test or one-way ANOVA followed by post-hoc Tukey's test. Significance threshold was $P<0.05$.

References
Anderson, H. C. (2003). Matrix vesicles and calcification. *Curr. Rheumatol. Rep.* **5**, 222-226.

Arratia, G., Schultze, H.-P. and Casciotta, J. (2001). Vertebral column and associated elements in dipnoans and comparison with other fishes: development and homology. *J. Morphol.* **250**, 101-172.

Begemann, G., Marx, M., Mebus, K., Meyer, A. and Bastmeyer, M. (2004). Beyond the neckless phenotype: influence of reduced retinoic acid signaling on motor neuron development in the zebrafish hindbrain. *Dev. Biol.* **271**, 119-129.

Bensimon-Brito, A., Cardeira, J., Cancela, M. L., Huysseune, A. and Witten, P. E. (2012). Distinct patterns of notochord mineralization in zebrafish coincide with the localization of Osteocalcin isoform 1 during early vertebral centra formation. *BMC Dev. Biol.* **12**, 28.

Bertrand, J., Cromme, C., Umlauf, D., Frank, S. and Pap, T. (2010). Molecular mechanisms of cartilage remodelling in osteoarthritis. *Int. J. Biochem. Cell Biol.* **42**, 1594-1601.

Bussmann, J. and Schulte-Merker, S. (2011). Rapid BAC selection for tol2-mediated transgenesis in zebrafish. *Development* **138**, 4327-4332.

Chou, C.-Y., Horng, L.-S. and Tsai, H.-J. (2001). Uniform GFP-expression in transgenic medaka (Oryzias latipes) at the F0 generation. *Transgenic Res.* **10**, 303-315.

Cooper, M. S., Szeto, D. P., Sommers-Herivel, G., Topczewski, J., Solnica-Krezel, L., Kang, H. C., Johnson, I. and Kimelman, D. (2005). Visualizing morphogenesis in transgenic zebrafish embryos using BODIPY TR methyl ester dye as a vital counterstain for GFP. *Dev. Dyn.* **232**, 359-368.

Curado, S., Anderson, R. M., Jungblut, B., Mumm, J., Schroeter, E. and Stainier, D. Y. R. (2007). Conditional targeted cell ablation in zebrafish: a new tool for regeneration studies. *Dev. Dyn.* **236**, 1025-1035.

DEVELOPMENT

Dale, R. M. and Topczewski, J. (2011). Identification of an evolutionarily conserved regulatory element of the zebrafish col2a1a gene. *Dev. Biol.* **357**, 518-531.

Dallas, S. L. and Bonewald, L. F. (2010). Dynamics of the transition from osteoblast to osteocyte. *Ann. N. Y. Acad. Sci.* **1192**, 437-443.

Doitsidou, M., Reichman-Fried, M., Stebler, J., Köprunner, M., Dörries, J., Meyer, D., Esguerra, C. V., Leung, T. C. and Raz, E. (2002). Guidance of primordial germ cell migration by the chemokine SDF-1. *Cell* **111**, 647-659.

Fleming, A., Keynes, R. and Tannahill, D. (2004). A central role for the notochord in vertebral patterning. *Development* **131**, 873-880.

Fleming, A., Kishida, M. G., Kimmel, C. B. and Keynes, R. J. (2015). Building the backbone: the development and evolution of vertebral patterning. *Development* **142**, 1733-1744.

Franz-Odendaal, T. A., Hall, B. K. and Witten, P. E. (2006). Buried alive: how osteoblasts become osteocytes. *Dev. Dyn.* **235**, 176-190.

Grotmol, S., Kryvi, H., Nordvik, K. and Totland, G. K. (2003). Notochord segmentation may lay down the pathway for the development of the vertebral bodies in the Atlantic salmon. *Anat. Embryol.* **207**, 263-272.

Grotmol, S., Nordvik, K., Kryvi, H. and Totland, G. K. (2005). A segmental pattern of alkaline phosphatase activity within the notochord coincides with the initial formation of the vertebral bodies. *J. Anat.* **206**, 427-436.

Huitema, L. F. A., Apschner, A., Logister, I., Spoorendonk, K. M., Bussmann, J., Hammond, C. L. and Schulte-Merker, S. (2012). Entpd5 is essential for skeletal mineralization and regulates phosphate homeostasis in zebrafish. *Proc. Natl. Acad. Sci. USA* **109**, 21372-21377.

Inohaya, K., Takano, Y. and Kudo, A. (2007). The teleost intervertebral region acts as a growth center of the centrum: in vivo visualization of osteoblasts and their progenitors in transgenic fish. *Dev. Dyn.* **236**, 3031-3046.

Jeradi, S. and Hammerschmidt, M. (2016). Retinoic acid-induced premature osteoblast-to-preosteocyte transitioning has multiple effects on calvarial development. *Development* **143**, 1205-1216.

Kague, E., Roy, P., Asselin, G., Hu, G., Simonet, J., Stanley, A., Albertson, C. and Fisher, S. (2016). Osterix/Sp7 limits cranial bone initiation sites and is required for formation of sutures. *Dev. Biol.* **413**, 160-172.

Kawakami, K. and Shima, A. (1999). Identification of the Tol2 transposase of the medaka fish Oryzias latipes that catalyzes excision of a nonautonomous Tol2 element in zebrafish Danio rerio. *Gene* **240**, 239-244.

Kroehne, V., Freudenreich, D., Hans, S., Kaslin, J. and Brand, M. (2011). Regeneration of the adult zebrafish brain from neurogenic radial glia-type progenitors. *Development* **138**, 4831-4841.

Kwan, K. M., Fujimoto, E., Grabher, C., Mangum, B. D., Hardy, M. E., Campbell, D. S., Parant, J. M., Yost, H. J., Kanki, J. P. and Chien, C.-B. (2007). The Tol2kit: a multisite gateway-based construction kit for Tol2 transposon transgenesis constructs. *Dev. Dyn.* **236**, 3088-3099.

Laue, K., Janicke, M., Plaster, N., Sonntag, C. and Hammerschmidt, M. (2008). Restriction of retinoic acid activity by Cyp26b1 is required for proper timing and patterning of osteogenesis during zebrafish development. *Development* **135**, 3775-3787.

Laue, K., Pogoda, H. M., Daniel, P. B., van Haeringen, A., Alanay, Y., von Ameln, S., Rachwalski, M., Morgan, T., Gray, M. J., Breuning, M. H. et al. (2011). Craniosynostosis and multiple skeletal anomalies in humans and zebrafish result from a defect in the localized degradation of retinoic acid. *Am. J. Hum. Genet.* **89**, 595-606.

LLeras Forero, L., Narayanan, R., Huitema, L. F. A., VanBergen, M., Apschner, A., Peterson-Maduro, J., Logister, I., Valentin, G., Morelli, L.G., Oates, A. and Schulte-Merker, S. (2018). Segmentation of the zebrafish axial skeleton relies on notochord sheath cells and not on the segmentation clock. *eLife* **7**, e33843.

Owen, R. (1866). Development of vertebrae. In *On the anatomy of vertebrates. Volume 1: Fishes and Reptiles*, pp. 30-34. Longmans, Green and Company.

Paavola, L. G., Wilson, D. B. and Center, E. M. (1980). Histochemistry of the developing notochord, perichordal sheath and vertebrae in Danforth's short-tail (sd) and normal C57BL/6 mice. *J. Embryol. Exp. Morphol.* **55**, 227-245.

Pennimpede, T., Cameron, D. A., MacLean, G. A., Li, H., Abu-Abed, S. and Petkovich, M. (2010). The role of CYP26 enzymes in defining appropriate retinoic acid exposure during embryogenesis. *Birth Defects Res. A Clin. Mol. Teratol.* **88**, 883-894.

Renn, J., Büttner, A., To, T. T., Chan, S. J. H. and Winkler, C. (2013). A col10a1: nlGFP transgenic line displays putative osteoblast precursors at the medaka notochordal sheath prior to mineralization. *Dev. Biol.* **381**, 134-143.

Scaal, M. (2016). Early development of the vertebral column. *Semin. Cell Dev. Biol.* **49**, 83-91.

Spoorendonk, K. M., Peterson-Maduro, J., Renn, J., Trowe, T., Kranenbarg, S., Winkler, C. and Schulte-Merker, S. (2008). Retinoic acid and Cyp26b1 are critical regulators of osteogenesis in the axial skeleton. *Development* **135**, 3765-3774.

To, T. T., Witten, P. E., Renn, J., Bhattacharya, D., Huysseune, A. and Winkler, C. (2012). Rankl-induced osteoclastogenesis leads to loss of mineralization in a medaka osteoporosis model. *Development* **139**, 141-150.

Waxman, J. S. and Yelon, D. (2011). Zebrafish retinoic acid receptors function as context-dependent transcriptional activators. *Dev. Biol.* **352**, 128-140.

Willems, B., Büttner, A., Huysseune, A., Renn, J., Witten, P. E. and Winkler, C. (2012). Conditional ablation of osteoblasts in medaka. *Dev. Biol.* **364**, 128-137.

Wopat, S., Bagwell, J., Sumigray, K. D., Dickson, A. L., Huitema, L. F. A., Poss, K. D., Schulte-Merker, S. and Bagnat, M. (2018). Spine patterning is guided by segmentation of the notochord sheath. *Cell Rep.* **22**, 2026-2038.

Yu, T., Graf, M., Renn, J., Schartl, M., Larionova, D., Huysseune, A., Witten, P. E. and Winkler, C. (2017). A vertebrate-specific and essential role for osterix in osteogenesis revealed by gene knockout in the teleost medaka. *Development* **144**, 265-271.

Zhou, Y., Cashman, T. J., Nevis, K. R., Obregon, P., Carney, S. A., Liu, Y., Gu, A., Mosimann, C., Sondalle, S., Peterson, R. E. et al. (2011). Latent TGF-beta binding protein 3 identifies a second heart field in zebrafish. *Nature* **474**, 645-648.

DEVELOPMENT